PAPER

Raman study of silicon telluride nanoplates and their degradation

To cite this article: Evan Hathaway *et al* 2022 *Nanotechnology* **33** 265703

IOP Publishing Nanotechnology
Nanotechnology 33 (2022) 265703 (9pp) https://doi.org/10.1088/1361-6528/ac5c13

Raman study of silicon telluride nanoplates and their degradation

Evan Hathaway[1], Jiyang Chen[2], Roberto Gonzalez-Rodriguez[1], Yuankun Lin[1] and Jingbiao Cui[1]

[1] Department of Physics, University of North Texas, Denton, TX 76203, United States of America
[2] Department of Physics and Material Science, University of Memphis, Memphis, TN 38152, United States of America

E-mail: jingbiao.cui@unt.edu

Received 16 November 2021, revised 31 January 2022
Accepted for publication 9 March 2022
Published 7 April 2022

Abstract

Silicon telluride (Si_2Te_3) has emerged as one of the many contenders for 2D materials ideal for the fabrication of atomically thin devices. Despite the progress which has been made in the electric and optical properties of silicon telluride, much work is still needed to better understand this material. We report here on the Raman study of Si_2Te_3 degradation under both annealing and *in situ* heating with a laser. Both processes caused pristine Si_2Te_3 to degrade into tellurium and silicon oxide in air in the absence of a protective coating. A previously unreported Raman peak at ~140 cm^{-1} was observed from the degraded samples and is found to be associated with pure tellurium. This peak was previously unresolved with the peak at 144 cm^{-1} for pristine Si_2Te_3 in the literature and has been erroneously assigned as a signature Raman peak of pure Si_2Te_3, which has caused incorrect interpretations of experimental data. Our study has led to a fundamental understanding of the Raman peaks in Si_2Te_3, and helps resolve the inconsistent issues in the literature. This study is not only important for fundamental understanding but also vital for material characterization and applications.

Keywords: silicon telluride, Raman spectroscopy, degradation

(Some figures may appear in colour only in the online journal)

1. Introduction

Research into two-dimensional materials continues to increase in popularity, driven by their unique electronic and optical properties along with their atomically thin structures. Despite this popularity, a few materials continue to dominate the field led by graphene and layered transition metal dichalcogenides such as MoS_2. The search for novel 2D materials as possible alternatives or improvements over current materials has played a key role in materials development. Recently, one such material which has emerged as a contender for use in 2D devices is silicon telluride (Si_2Te_3) [1–4].

Si_2Te_3 is an intrinsic p-type semiconducting material with a unique layered trigonal structure, with silicon dimers occupying two-thirds of the octahedral vacancies created between HCP Te atoms [5, 6]. Each Te–Si–Te layer is separated by van der Waals forces making mechanical exfoliation possible. Silicon dimers may take on one of four possible orientations leading to changes in the electronic and optical properties [7], offering the unique opportunity to control the material properties through the manipulation of dimer orientations. Recent studies have also shown Si_2Te_3 to have potential applications in 2D transistor devices, broadband photodetectors, and resistive memory devices [1, 8, 9].

It is well known that silicon telluride is not environmentally stable under ambient conditions, characterized by its stark red color turning black over the course of a few hours to days. This degradation was, to our knowledge, first explained by Bailey [10] and later confirmed by others [1, 5, 11] and was found to be due to Si_2Te_3 reaction with moisture in the air, resulting in the formation of hydrated silicon dioxide and hydrogen telluride, the latter of which spontaneously degrades into hydrogen and tellurium. Despite this fact, little has been done to better understand the degradation so as to make it possible to probe the material stability for device applications.

Raman spectroscopy is a key technique used to study Si_2Te_3 and other 2D materials. The typical Raman peaks for Si_2Te_3 are located at $\sim$120 cm^{-1} and $\sim$144 cm^{-1} and have been assigned as the A^1_{1g} and A^2_{1g} modes respectively by some researchers [8, 12, 13]. The A^2_{1g} mode is well understood to be a result of symmetric out-of-plane stretching [14] while no conclusive data exist which explain the origin of the A^1_{1g} mode, which was assigned as such based solely from polarised Raman measurements [12].

The reported A^1_{1g} peak intensity is inconsisitent in the literature and varies from group to group and even from sample to sample within the same research group. This variability has been attributed to sample thickness [8], defects [13], and dopant concentrations [12] in previous works, and has led many to conclude that degraded samples of Si_2Te_3 with strong Raman peak at $\sim$120 cm^{-1} are pristine [1, 4, 12, 13, 15]. These modes have been considered a signature feature of Si_2Te_3 for evaluating the quality of the material.

In this study, however, we find the A^1_{1g} peak to actually be the A_1 peak of crystalline tellurium, which was incorrectly assigned to Si_2Te_3 in some of the literature. The A_1 mode's variablility can be explained by the variable thickness of tellurium which accumulates at the surface as a result of the hydrolysis process. We also find the A^2_{1g} mode actually contains two peaks at 140 cm^{-1} and 144 cm^{-1}, belonging to the E_2 mode of tellurium and A_{1g} mode (previously labeled as the A^2_{1g} mode) of Si_2Te_3 respectively. The A_1 mode of crystalline tellurium is caused by symmetric chain expansion within the basal plane, while the E_2 mode is primarly due to asymmetric stretching along the *c*-axis [16, 17].

It was observed that the A_{1g} mode of Si_2Te_3 decreases and is overtaken by the very closely spaced E_2 mode of tellurium when the Si_2Te_3 samples degrade. Our experimental data has led to a fundamental understanding of the origin of the Raman peaks in Si_2Te_3, which helps to resolve the inconsistent issues in the literature and provides the correct physics behind those experiments. Lastly, we demonstate an effective way to prevent the degradation of Si_2Te_3 by depositing a thin protection layer of Al_2O_3 by atomic layer deposition (ALD). This protective coating is shown to provide long term stability of the material for device applications.

2. Experimental methods

2.1. Sample preparation

Nanoplates of Si_2Te_3 were grown on silicon substrates using a CVD process. Full experimental details can be found in previous publications [4]. In short, tellurium and silicon powdered precursors are put upstream in a heated tube furnace. A nitrogen carrier gas is flown through the tube, transporting the evaporated precursors, and depositing them on downstream silicon wafers or other substrates. The thickness of the nanoplates varies from tens of nanometers to hundreds of nanomaters, depending on the growth conditions. Those samples used in this study have thicknesses around 500 nm. The as-deposited samples were then characterized and subsequently stored in a vacuum chamber to avoid degradation. In order to protect the samples, a 50 nm Al_2O_3 coating was deposited over the Si_2Te_3 nanoplates at 150 °C via a Savannah S100 ALD system. The deposition was achieved using alternating 0.015 s pulses of trimethylaluminum and water transported via a nitrogen carrier gas flowing at 20 sccm.

2.2. Controlled degradation through in situ laser heating

Degradation can be induced by heating the sample *in situ* through controled laser exposure. High laser power and/or long exposure times will degrade the exposed area of the Si_2Te_3 nanoplates due to local laser heating. Raman and photoluminescence (PL) spectra were taken in quick succession with only a few seconds of pause between each measurement. Raman and PL spectroscopy were performed using a Renishaw InVia Raman Microscope with a 532 nm wavelength laser. The spectra were collected from the same position on the sample with laser powers of 0.25 mW and 0.5 mW and a 1.0 s exposure time for Raman measurements and a laser power of 25 μW and an exposure time of $\sim$2 min for PL measurements. This procedure allows for more control over the speed of degradation and confines the degradation to the area of the laser spot. It also guarantees the spectra are taken from the exact same spot on the sample.

2.3. Controlled degradation through annealing

A controlled degradation process was performed by annealing Si_2Te_3 nanoplates at varying temperatures. Samples were placed into the reaction chamber of a Savannah S100 ALD system, where they were then annealed in air at temperatures ranging from 50 °C to 300 °C for a duration of 5 min at each temperature. Samples were then allowed to cool to room temperature before a Raman spectrum was taken. The laser power was set to 25 μW and the exposure time was 1.0 s for each measurement to avoid degradation due to laser heating during Raman measurement.

2.4. SEM and EDS measurements

The morphology and composition of the sample was characterized using a FEI Quanta 200 environmental scanning electron microscopy (SEM) with energy dispersive spectroscopy (EDS). SEM and EDS measurements were carried out after samples were annealed following the process outlined above. The same nanoplate was characterized by SEM and EDS along with Raman measurement.

2.5. Polarised raman measurements

Polarized Raman measurements were carried out using the Renishaw polariser/analyser kit for the inVia Raman microscope. The kit consists of a polarisor and half-wave plate (the analyser) which can be inserted into the path of the scattered light in order to control the polarisation of the collected spectra. The laser has an inherent vertical polarisation and so

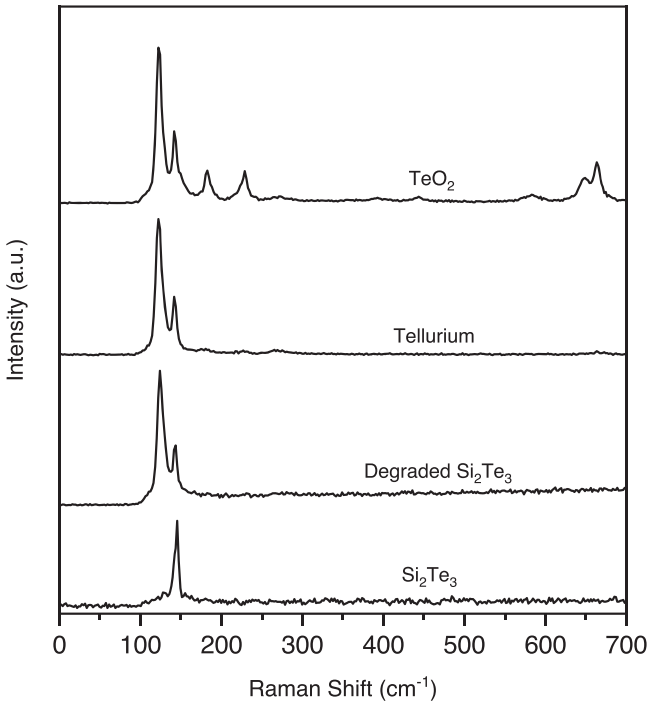

Figure 1. Raman spectra of pristine Si_2Te_3, degraded Si_2Te_3, tellurium, and TeO_2.

without the polarisor or analyser inserted into the beam path the 'Porto notation' for the Raman scattering of this configuration is $z(x, -)\bar{z}$. In this configuration light is incident (z) and scattered($\bar{z}$) along the z direction, the incident light (x) is polarised in the x direction, and the collected scattered light ($-$) is unpolarised. With the polarisor inserted, the configuration changes to $z(x, x)\bar{z}$, and the incident and collected scattered light are parallel to one another. If the polarisor and the analyser are both inserted into the beam path the configuration becomes $z(x, y)\bar{z}$ and the incident and collected scattered light are perpendicular to one another. Comparing the Raman peak intensities in these parallel and perpendicular configurations can determine the symmetry of the vibrational modes which lead to the Raman peaks seen in the measurements.

3. Results and discussion

Figure 1 shows a comparison of Raman spectra taken from pristine Si_2Te_3, degraded Si_2Te_3, pure tellurium, and TeO_2. The difference in Raman spectra for Si_2Te_3 and degraded Si_2Te_3 is clear, marked by the emergence of a peak at $\sim$120 cm^{-1}, which has been previously assigned as the A^1_{1g} mode [12]. Also, it is clear from this image that the Raman spectrum for degraded Si_2Te_3 matches closely that of pure tellurium. This is consistent with the findings of Bailey [10], who suggested that pure tellurium is a by product of the degradation process. Therefore, it is likely that what has previously been assigned as an A^1_{1g} mode of Si_2Te_3 is actually the A_1 mode for tellurium. The freshly grown and pristine Si_2Te_3 has only one significant Raman peak at 144 cm^{-1}, while most of Raman data in the literature typically show two primary peaks, indicating the samples are degraded Si_2Te_3 containing tellerium.

TeO_2 has many polymorphs. The Raman spectrum shown in figure 1 is likely the α polymorph obtained by exposing tellurium to a high laser intensity [18]. This polymorph has ten prominent Raman peaks, two of which it shares with pure Te located at 120 and 140 cm^{-1}, and eight more higher energy peaks located at 182, 229, 273, 394, 444, 581, 664, and 684 cm^{-1}. It should be noted that degraded Si_2Te_3 does not show any of these higher energy peaks and so it is unlikely that the change in the Raman spectra between pristine and degraded samples is due to the formation of TeO_2.

In order to study the details of the Raman spectral change of Si_2Te_3 during the degradation process, a controlled experiment was carried out using successive laser exposure of a nanoplate in air. The details of this process can be found in experimental methods. Figure 2(a) shows the successive Raman spectra taken from a Si_2Te_3 nanoplate at a laser power of 0.5 mW. The assignment of the Raman peaks are labelled on the figure as the A_1 and E_2 modes of tellurium and A_{1g} of Si_2Te_3. The freshly grown sample shows a very small peak at $\sim$120 cm^{-1} and a more pronounced peak at $\sim$144 cm^{-1} with a slight shoulder on its left hand side. As the cumulative laser exposure of the sample increases the Raman peak at $\sim$120 cm^{-1} also increases, and what was initially a slight shoulder at $\sim$140 cm^{-1} becomes more pronounced until, after 15 s of cumulative laser exposure, it completely dominates the peak located at $\sim$144 cm^{-1}. This is evidence that what was thought to be a single peak located at $\sim$144 cm^{-1} is actually two peaks which are closely spaced about 3–4 cm^{-1} apart. This close spacing along with the weak signal of the peak at $\sim$140 cm^{-1} for nearly pristine Si_2Te_3 may be the reasons why this peak had previously gone unnoticed by many researchers.

To illustrate the fine spectral change, the Raman peaks in figure 2(a) were deconvoluted using a Lorentzian function. A typical deconvolution spectrum for the laser exposure time of 7 s is demonstrated in figure 2(b). The experimental data can be well fit by three peaks at 120 cm^{-1}, 140 cm^{-1}, and 144 cm^{-1}.

The peak intensities (areas) of the deconvoluted peaks were plotted as a function of the cumulative laser exposure time in figure 2(c). From this graph, one can see that the fastest change in the peak intensity occurs before 6 s of cumulative laser heating. Both the A_1 and E_2 peaks of tellurium dramatically increase while the A_{1g} peak of Si_2Te_3 decreases rapidly during the initial *in situ* heating by the laser. The E_2 peak of tellurium overtakes the A_{1g} peak of Si_2Te_3 at about 4 s of laser exposure. After a laser exposure of 8 s the peak intensities show only slight changes, likely because most of the Si_2Te_3 has degraded to tellurium. Also of note, is that the penetration depth of a 532 nm laser in tellurium can be calculated from the known complex index of refraction [19] to be $\sim$14.7 nm. This small penetration depth means that it is also possible the thin top layer of tellurium formed after successive laser exposure protects the Si_2Te_3 beneath from

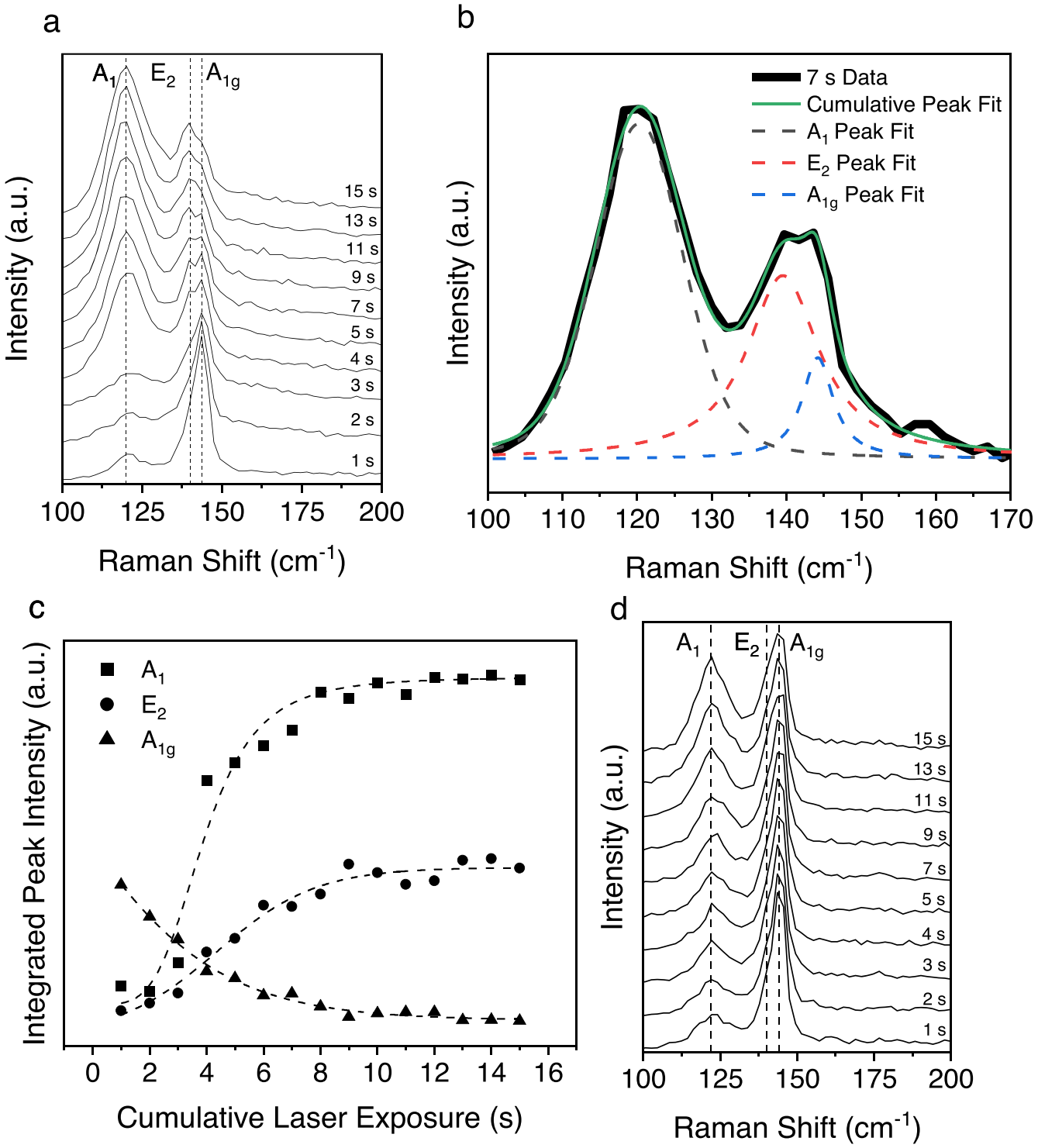

Figure 2. (a) Raman spectra of Si_2Te_3 nanoplate after successive *in situ* laser heating at a power of 0.5 mW. The spectra are offset vertically for readability. (b) Deconvolution of a Raman spectrum taken after 7 s of laser exposure at 0.5 mW. (c) Integrated Raman peak intensity as a function of laser exposure time at a power of 0.5 mW. The dashed lines are drawn to guide the eyes. (d) Raman spectra of Si_2Te_3 nanoplate after successive *in situ* laser heating at a power of 0.25 mW.

further degradation by limiting the penetration depth of the laser.

Figure 2(d) shows successive Raman measurements taken with a laser power of 0.25 mW instead of 0.5 mW of the same nanoplate. After 15 s of cumulative laser exposure from the 0.25 mW laser, the A_1 peak is still smaller than the A_{1g} peak, indicating the sample is only moderately degraded. This is quite different from the same sample after 15 s of cumulative laser exposure from the 0.5 mW laser, which shows the A_1 peak much larger than the A_{1g} peak.

From these data it is clear that Si_2Te_3 is very sensitive to both the exposure time and intensity of the laser, which can be

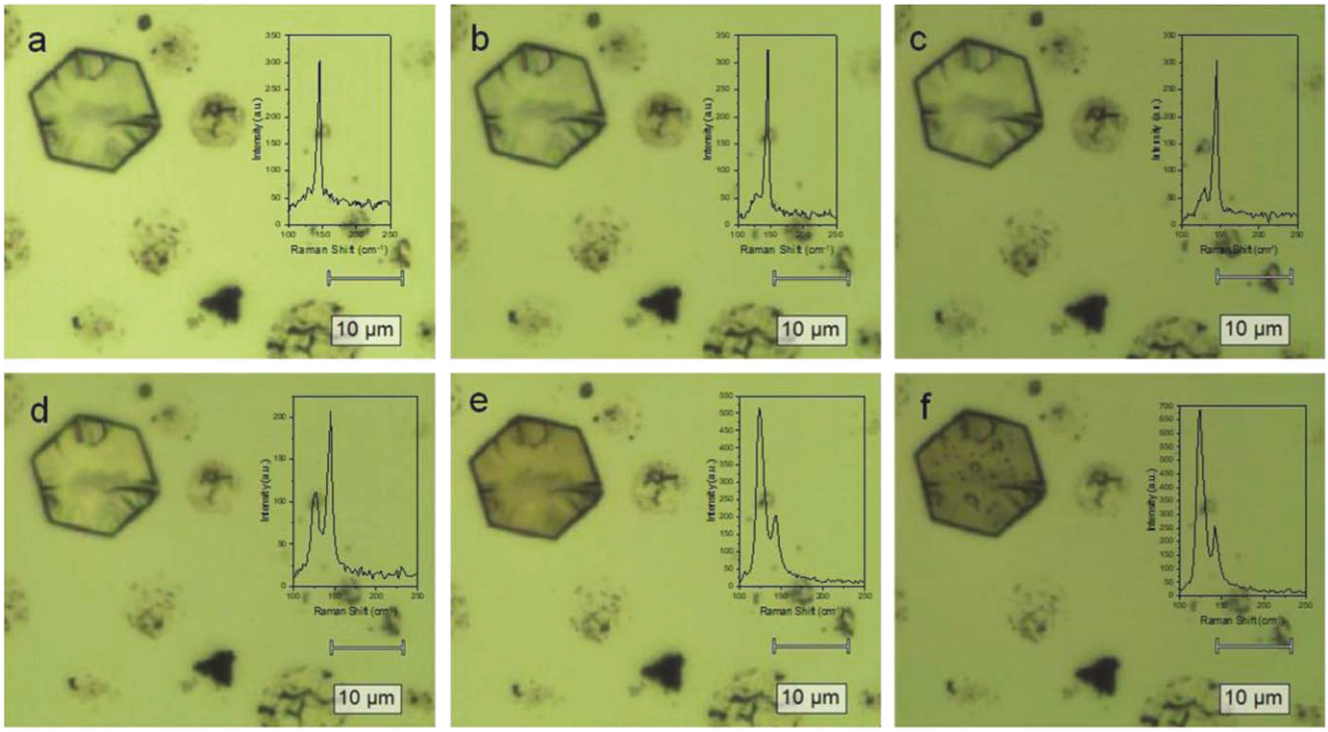

Figure 3. Optical images and Raman spectra taken after the sample was annealed at temperatures of (a) 25 °C, (b) 50 °C, (c) 100 °C, (d) 150 °C, (e) 200 °C, and (f) 250 °C respectively.

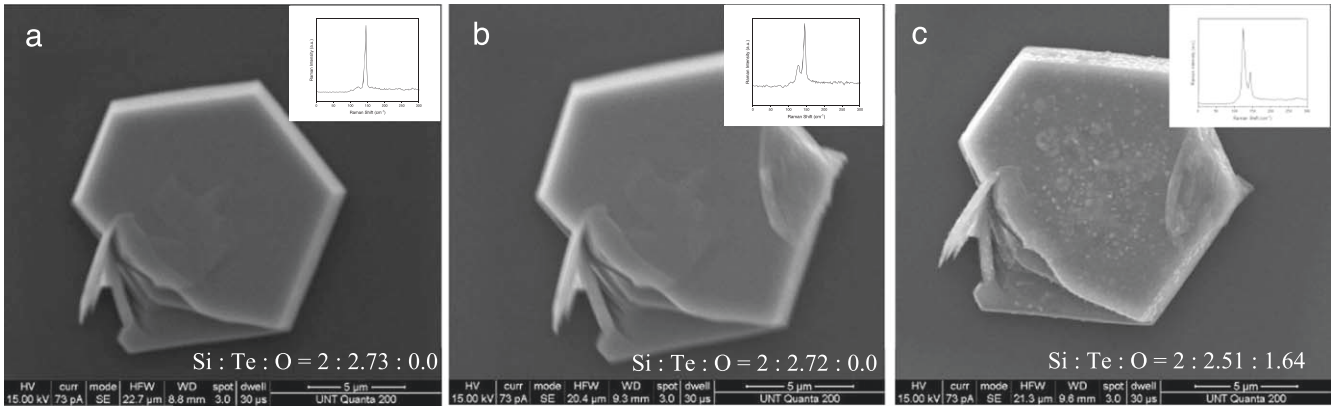

Figure 4. SEM images, Raman spectra, and atomic ratios for Si_2Te_3 samples anealed at (a) 25 °C, (b) 150 °C, and (c) 300 °C respectively.

used to study the degradation with finer control and on shorter time scales than other methods. However, this also means that one needs to be cautious when taking any measurements which involve the use of a laser. The exposure time and laser intensity must be very carefully chosen or must be done in a moisture free environment, otherwise there is a strong risk of unintentional degradation.

It has been shown that many other tellurium containing 2D nanostructured materials, such as GaTe, $ZrTe_3$, CdTe, and ZnTe, degrade in a similar way to that shown in figure 2, marked by the emergence of two Raman peaks located at $\sim$120 cm^{-1} and $\sim$140 cm^{-1} as samples age [20, 21]. Yang *et al* [20] found this degradation in GaTe and $ZrTe_3$ to be caused by the oxidation of tellurium atoms after interacting with H_2O in the air, resulting in the formation of TeO_2. Tellurium, however, is known to resist oxidation under ambient conditions and, as shown in figure 1, the resulting Raman spectrum does not match any known polymorph of TeO_2 [18], and so this explanation for Si_2Te_3 is questionable. Instead, the peaks which emerge after degradation in figure 2(a) more closely resemble those of pure tellurium, with the peaks located at 120 cm^{-1} and 140 cm^{-1} being identical to the A_1 and E_2 modes of crystalline tellurium [17, 22]. As such, we conclude that Si_2Te_3 degrades into tellurium and silicon oxides. These findings are more in line with the conclusions of Larramendi *et al* [21] ,who found the degradation as a function of laser intensity of ZnTe into Te to be photochemical in nature and likely thermally activated.

To further study the change in the Raman spectra of degraded Si_2Te_3, another controlled degradation process was carried out by annealing nanoplates of Si_2Te_3 at progressively higher temperatures. Figure 3 shows the optical images and

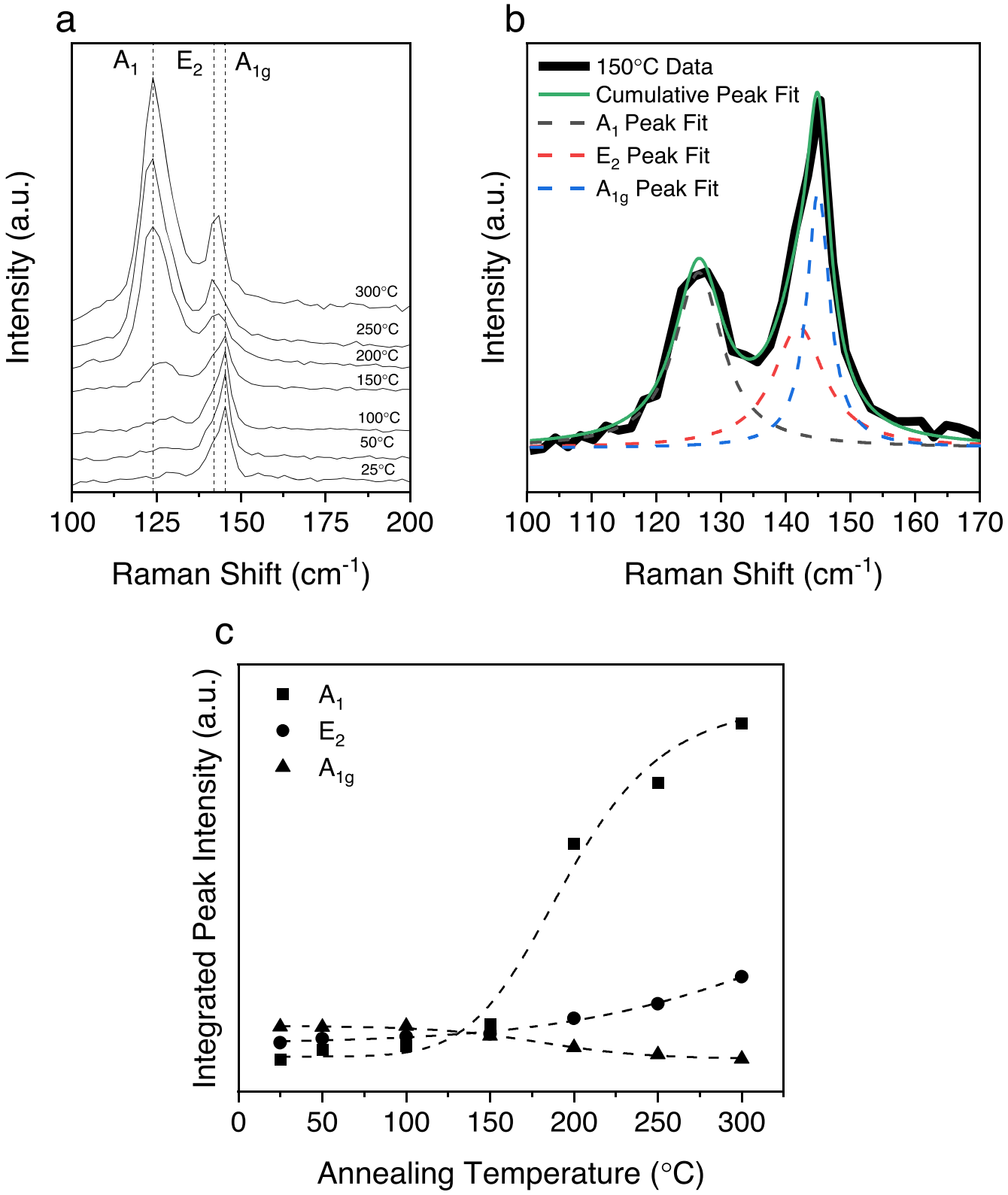

Figure 5. (a) Raman spectra of Si_2Te_3 after being annealed for 5 min at varying temperatures. (b) Deconvolution of the Raman spectrum taken after the 150 °C annealing step. (c) Integrated Raman peak intensity as a function of annealing temperature.

Raman spectra of a nanoplate after each step of the annealing process described in experimental methods. It is obvious upon studying the insets of figure 3, that the A_1 peak drastically increases as the sample's annealing temperature is increased up to 150 °C. It should be noted that significant degradation occurs after annealing at 150 °C, even though a change in the color and morphology are not noticable between figures 3(c) and (d). Because of this, care must be taken not to

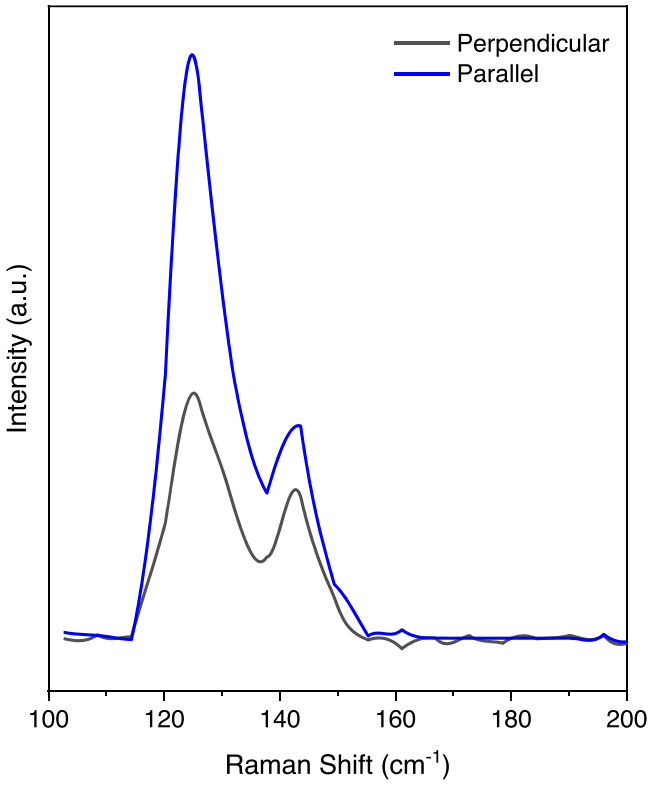

Figure 6. Polarized Raman spectra of degraded Si_2Te_3 nanoplate.

mischaracterize degraded Si_2Te_3 as pristine solely based off the color and morphology of the sample.

EDS measurements were taken of a Si_2Te_3 nanoplate to investigate the compositional change in the annealed samples. Figure 4 shows the SEM images along with the Raman spectra taken after being annealing at 25 °C, 150 °C, and 300 °C. The atomic ratios of Si:Te:O on figure 4 were obtained from EDS measurements. The atomic ratio for the unannealed sample is 2:2.73:0, which is close to the expected stoichiometry of Si_2Te_3. This value remains unchanged after the sample was annealed at 150 °C even though the Raman spectrum indicates an increase of A_1 peak of tellurium, likely due to the insensitivity of EDS measurements to the very small amount of oxygen. However, figure 4(c) shows a dramatic change in composition marked by an increase in oxygen along with a remarkable change in the surface morphology and Raman spectrum. The tellurium content decreases in the sample annealed at 300 °C, likely due to the evaporation of some of the Te from the surface during the annealing process. These results verify that the annealing of the sample causes oxidation of silicon atoms following hydrolysis.

Figure 5 allows for a more careful examination of the spectra included in the insets of figure 3. Here, the results are consistent with the succesive laser measurements, showing that the A_1 and E_2 tellurium peaks increase while the A_{1g} Si_2Te_3 peak decreases as the annealing temperature increases. Note that up to a temperature of 100 °C, the annealing only causes very small changes in the Raman spectra. The spectra were again deconvoluted using Lorentzian functions as demonstrated in figure 5(b) for the spectrum taken after annealing at 150 °C. The spectrum can be well fit with the A_1 and E_2 modes of Te and the A_{1g} mode of Si_2Te_3. The peak intensities as a function of annealing temperature are plotted in figure 5(c). Similar to what we have observed in figure 2 for the *in situ* laser heating, the peak intensities of Te increase while that of Si_2Te_3 decreases as the annealing temperature increases. The A_{1g} peak remains reletively constant until after the 150 °C annealing step, where it begins to be dominated by the increasing E_2 peak.

To further confirm the Raman peaks which emerge after degradation are in fact the A_1 and E_2 peaks of crystalline tellurium, polarized Raman measurements were carried out as described in experimental methods. The Raman spectra were taken from a degraded Si_2Te_3 sample at different polarization configurations. It is generally known that light scattered from symmetric vibrational modes retains the polarization of the incident light, while light scattered from asymmetric modes does not. By controlling the polarisation of the incident and collected scattered light, it is possible to identify which Raman peaks are from symmetric or asymmetric vibrational modes. When the incident light has a polarization perpendicular to the scattered light you would expect to see a large reduction in the Raman peak intensity for the symmetric modes while the asymmetric modes will be less effected. It has been shown that the depolarization ratio, defined as the perpendicular peak intensity divided by the parallel peak intensity, is greater than 0.75 for asymmetric (depolarized) modes and less than 0.75 for symmetric (polarized) modes [23].

Figure 6 shows the Raman spectra taken from a degraded Si_2Te_3 nanoplate in both the parallel and perpendicular polarization configurations. The intensities of each peak were recorded and used to calculate the depolarization ratios, which were found to be 0.41 and 0.81 for the A_1 and E_2 modes respectively. This is consistent with the A_1 mode being symmetric and the E_2 mode being asymmetric, matching other results found for crystalline tellurium [22]. Thus, the assignment of A_1 and E_2 peaks to tellurium in the Raman spectra of degraded Si_2Te_3 is further confirmed.

The degradation of Si_2Te_3 nanoplates with an Al_2O_3 protective coating was studied by Raman and photoluminescence spectroscopy. A 50 nm thick layer of Al_2O_3 was deposited over the Si_2Te_3 nanoplates via ALD in an effort to insulate the sample from moisture in the air. Both traditional annealing and *in situ* laser heating were carried out for the coated samples.

Figure 7 shows Raman and PL measurements for laser induced degradation of uncoated and Al_2O_3 coated Si_2Te_3. The times shown in figure 7 are the cumulative laser exposure time after each successive measurement. Due to the extended exposure time that is needed for PL measurement, a much lower laser power of 25.0 μW was used for this experiment. One can see that the uncoated sample shown in figure 7(a) rapidly degraded, evidenced by the increase in the A_1. This observation is similar to that made of figure 2. The corresponding photoluminescence spectra shown in figure 7(b) have a broadband emission from the defects in Si_2Te_3, which is

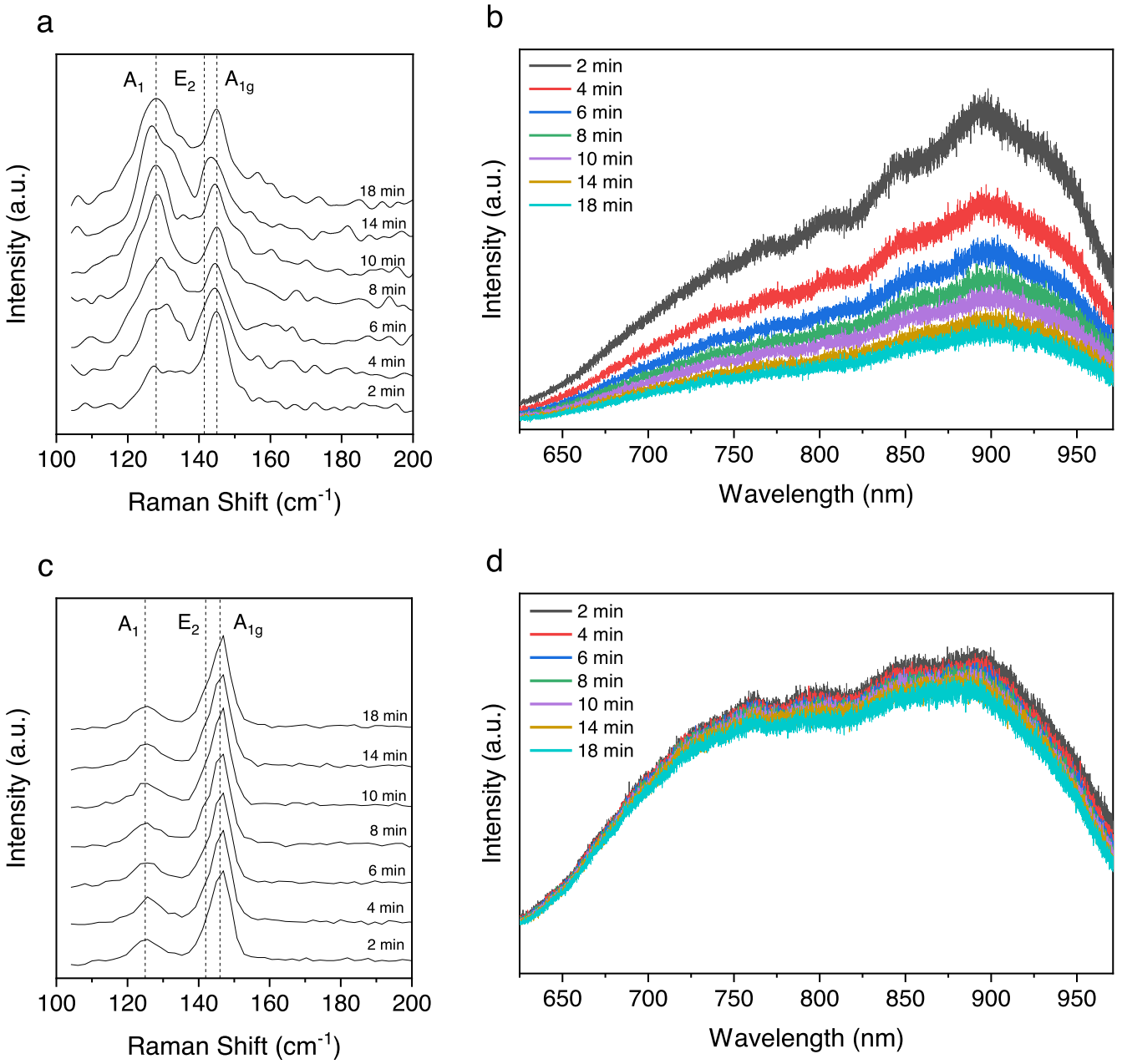

Figure 7. Raman and PL spectra of both uncoated and coated Si_2Te_3 samples. (a) Successive Raman spectra of uncoated Si_2Te_3. (b) Successive photoluminescence spectra of uncoated Si_2Te_3. (c) Successive Raman spectra of coated Si_2Te_3. (d) Successive photoluminescence spectra of coated Si_2Te_3.

similar to previously reported data [4]. The PL emission intensity decreases after increasing laser exposure. This is easy to understand because the laser heating has converted the Si_2Te_3 to tellurium and silicon oxide as has been discussed in the previous paragraphs.

Figure 7(c) and (d) show the corresponding Raman and PL spectra taken of the coated Si_2Te_3 after successive laser exposure. The laser power was kept the same as the experiment for the uncoated sample for comparison. Both the Raman and PL spectra of the coated sample remain stable after the laser exposure, demonstrating that the Si_2Te_3 material did not degrade during the laser exposure, which is drastically different from the uncoated sample. The PL intensity shows a slight decrease, but the Raman shows no noticeable change. The traditional annealing experiment on the coated Si_2Te_3 sample was also carried out from room temperature to 300 °C. The Raman spectra showed no obvious change in peak shape and intensity, which is consistent with the *in situ* laser heating and again confirms that the coated Si_2Te_3 sample is stable even at high temperature.

4. Conclusion

Silicon telluride and its degradation are studied by Raman spectroscopy. The pristine Si_2Te_3 has a signature A_{1g} Raman

peak at 144 cm^{-1}. However, the material is sensitive to moisture in air and may experience a change in property even during Raman measurement. Controlled degradation by both annealing and *in situ* laser heating have been employed in this study. After degradation, the A_1 and E_2 Raman modes of tellurium are observed. The E_2 mode of Te is very close to the A_{1g} mode of Si_2Te_3 and has been incorrectly assigned to Si_2Te_3 in the literature. This study helps to clarify this ambiguity and lead to better understanding of Si_2Te_3 in terms of its signature Raman mode. The degradation study of the coated sample with a thin protection layer shows that a thin coating is effective at preventing Si_2Te_3 from degrading even at temperatures of 300 °C in air.

Acknowledgments

This research was partially supported by the U.S. National Science Foundation with grant numbers 2128367 and 1709528.

Data availability statement

The data that support the findings of this study are available upon reasonable request from the authors.

ORCID iDs

Roberto Gonzalez-Rodriguez https://orcid.org/0000-0001-6849-1799
Jingbiao Cui https://orcid.org/0000-0003-3408-1016

References

[1] Keuleyan S, Wang M, Chung F R, Commons J and Koski K J 2015 *Nano Lett.* **15** 2285–90
[2] Rick M, Rosenzweig J and Birkholz U 1984 Anisotropy of electrical conductivity in Si_2Te_3 *Phys. Status Solidi* (a) **83** K183–6
[3] Chen J *et al* 2020 Anisotropic optical properties of single Si2Te3 nanoplates *Sci Rep.* **10** 19205
[4] Wu K, Sun W, Jiang Y, Chen J, Li L, Cao C, Shi S, Shen X and Cui J 2017 Structure and photoluminescence study of silicon based two-dimensional Si_2Te3 nanostructures *J. Appl. Phys.* **122** 075701
[5] Rick M, Rosenzweig J and Birkholz U 1984 Anisotropy of electrical conductivity in Si_2Te_3 *Phys. Status Solidi* (a) **83** K183–6
[6] Gregoriades P E, Bleris G L and Stoemenos J 1983 *Acta Crystallogr.* B **39** 421–6
[7] Shen X, Puzyrev Y S, Combs C and Pantelides S T 2016 Variability of structural and electronic properties of bulk and monolayer Si_2Te_3 *Appl. Phys. Lett.* **109** 113104
[8] Chen J W, Tan C Y, Li G, Chen L J, Zhang H L, Yin S Q, Li M, Li L and Li G H 2021 2D silicon-based semiconductor Si_2Te_3 toward broadband photodetection *Small* **17** 2006496
[9] Wu K, Chen J, Shen X and Cui J 2018 Resistive switching in Si_2Te_3 nanowires *AIP Adv.* **8** 125008
[10] Bailey L G 1966 Preparation and properties of silicon telluride *J. Phys. Chem. Solids* **27** 1593–8
[11] Rau J W and Kannewurf C R 1966 Intrinsic absorption and photoconductivity in single crystal SiTe2 *J. Phys. Chem. Solids* **27** 1097–101
[12] Wang M, Lahti G, Williams D and Koski K J 2018 *ACS Nano* **12** 6163–9
[13] Johnson V L, Anilao A and Koski K J 2019 Pressure-dependent phase transition of 2D layered silicon telluride (Si_2Te_3) and manganese intercalated silicon telluride *Nano Res.* **12** 2373–7
[14] Zwick U and Rieder K H Z 1976 *Physica* B **25** 319–22
[15] Song X, Ke Y, Chen X, Liu J, Hao Q, Wei D and Zhang W 2020 *Nanoscale* **12** 11242
[16] Martin R M, Lucovsky G and Helliwell K 1976 *Phys. Rev.* B **13** 1383
[17] Du Y, Qiu G, Wang Y, Si M, Xu X, Wu W and Ye P D 2017 *Nano Lett.* **17** 3965–73
[18] Mirgorodsky A, Merle-Mejean T, Champarnaud J-C, Thomas P and Frit B 2000 Dynamics and structure of TeO_2 polymorphs: model treatment of paratellurite and tellurite; Raman scattering evidence for new γ- and δ-phases *J. Phys. Chem. Solids* **61** 501–9
[19] Ciesielski A, Skowronski L, Pacuski W and Szoplik T 2018 Permittivity of Ge, Te and Se thin films in the 200–1500 nm spectral range. Predicting the segregation effects in silver *Mat. Sci. Semicond. Process.* **81** 64–7
[20] Yang S *et al* 2017 Environmental stability of 2D anisotropic tellurium containing nanomaterials: anisotropic to isotropic transition *Nanoscale.* **9** 12288–94
[21] Larramendi E M *et al* 2010 *Semicond. Sci. Technol.* **25** 075003
[22] Pine A and Dresselhaus G 1971 Raman spectra and lattice dynamics of tellurium *Phys. Rev.* B **4** 356–71
[23] Allemand C D 1970 Depolarization ratio measurements in raman spectrometry *Appl. Spectrosc.* **24** 348–53